PHYSICAL REVIEW D **93,** 015004 (2016)

Vector boson scattering at the LHC: A study of the $WW \to WW$ channels with the Warsaw cut

M. Fabbrichesi,[1] M. Pinamonti,[2,3] A. Tonero,[4] and A. Urbano[1,3]

[1]*INFN, Sezione di Trieste, via Valerio 2, 34127 Trieste, Italy*
[2]*INFN, Gruppo collegato di Udine, Sezione di Trieste, via Valerio 2, 34127 Trieste, Italy*
[3]*SISSA, via Bonomea 265, 34136 Trieste, Italy*
[4]*ICTP-SAIFR, Rua Dr. Bento Teobaldo Ferraz 271, 01140-070 São Paulo, Brazil*

(Received 2 October 2015; published 8 January 2016)

We study W boson scattering in the same- and opposite-sign channels under the assumption that no resonances are present in the collider processes $pp \to l^\pm \nu_l l^\pm \nu_l jj$ and $pp \to l^\pm \nu_l l^\mp \nu_l jj$, respectively. Basic selection cuts together with a restriction on the combination of the final lepton and jet momenta (the Warsaw cut) make it possible to argue that at the LHC a luminosity of 100 fb^{-1} and a center-of-mass energy of $\sqrt{s} = 13$ TeV will allow us to constrain the leading effective Lagrangian coefficients at the permil level. We also discuss limits on the other coefficients of the effective Lagrangian as well as stronger constraints provided by higher energy and luminosity.

DOI: 10.1103/PhysRevD.93.015004

I. INTRODUCTION

Vector boson scattering (VBS) at the LHC provides a direct window on the mechanism responsibile for the breaking of the electroweak (EW) symmetry. The tree-level amplitude for VBS is the combination of seven subprocesses in which gauge and Higgs bosons are exchanged. In the standard model (SM), the terms leading in energy cancel, leaving an amplitude and a cross section consistent with unitary. If any or all among the trilinear and quartic gauge couplings and the Higgs boson coupling to the vector bosons are modified, these delicate cancellations fail, and tree-level unitarity is lost. In particular, if either the trilinear or the quartic gauge couplings are changed, terms proportional to the fourth power of the c.m. energy will be present.

After the existence of the Higgs boson has been confirmed [1], we know that this particle plays a role in EW symmetry breaking, but the details may differ from the basic scenario in which the Higgs boson is linearly and minimally coupled. If the gauge couplings are left unchanged but the Higgs boson couplings to the vector bosons are modified, terms proportional to the square of the c.m. energy will be present in the amplitude for VBS.

All these potential departures from the SM represent signals for new physics. Since there are many possibilities—ranging from an extended Higgs sector to strong dynamics—they are best described by means of an effective field theory.

Terms in the amplitude growing with the c.m. energy arise when considering the scattering among the longitudinal components of the vector bosons. Using the equivalence theorem [2], these components can be identified with the Goldstone bosons of the EW symmetry breaking and behave as scalar particles with derivative couplings: their scattering amplitudes are similar to those for $\pi\pi$ scattering in QCD, and the same techniques can be used. The transverse components give rise to terms in the amplitude that are not growing with the c.m. energy and therefore they can be considered subleading—for all practical purposes, they are part of the background. The natural language for computing the relevant amplitudes is that of the effective nonlinear (chiral) EW Lagrangian first introduced in Ref. [3].

Depending on the symmetry group used, there exist different effective Lagrangians which are equivalent but differ in the order-by-order terms and therefore in the dimension and field content of the operators. Compared to other effective Lagrangians based on the linear theory and the full symmetry group, the chiral EW Lagrangian has the advantage of being optimized for VBS.

The loss of tree-level unitarity suggests the presence of a strongly interacting sector. We expect unitarity to be restored by the presence of resonances. Barring the spectacular case of the LHC actually seeing one or more of these resonances, this loss and its eventual restoration can be studied by the effective EW Lagrangian in terms of bounds of its coefficients. Because we now know that the theory also contains a Higgs boson, such a Lagrangian must be completed by the introduction of this field [4,5]—the effect of which is parametrized in terms of additional coefficients.

The same-sign $W^\pm W^\pm \to W^\pm W^\pm$ channel stands out in this search because of the suppressed QCD background and the reduced contribution from channels where transverse and longitudinal gauge bosons are mixed. It is a channel in which it is easier to single out the scattering of the longitudinal components of the gauge bosons and the most likely place to look for possible deviations from the SM.

Possible resonances in this channel are expected to be either present in the t channel (and therefore leading to only a decrease of the cross section) or carrying isospin 2 and doubly charged and therefore heavier than those in other decay channels. Under the assumption that no resonance has been seen in this or other channels, it is reasonable to unitarize the amplitude by the simplest and model-independent means without worrying about the value of the resonances' masses and widths. Experimental cross sections for the process $pp \to l^\pm \nu_l l^\pm \nu_l jj$ can then be compared with the SM and provide the means to constrain the coefficients of the effective Lagrangian and the physics behind the EW symmetry breaking.

Even in the same-sign WW channel, the extraction of the coefficients is challenging. Appropriated selection cuts are required to isolate the VBS process from other, often larger backgrounds. In addition, we want to isolate the longitudinally from the transversally polarized vector boson. The former is mostly produced together with a final quark, which is more forward than in the case in which the W is transversally polarized. These requirements provide a standard set of selection rules to which we add a final requirement (the Warsaw cut [6]) on the size and direction of the final transverse momenta of jets and leptons which has been shown to be effective in disentangling longitudinal and transverse vector boson polarizations.

The opposite-sign $W^\pm W^\mp \to W^\pm W^\mp$ channel is less clean mainly because of the large background generated by the production of $t\bar{t}$ pairs. It would be best to do without it. Whereas we find that it is possible to establish the most stringent constraints by means of only the same-sign channel if the coefficients are varied one at the time, both channels are required if the coefficients are varied simultaneously.

The study of the cross sections $\sigma(pp \to l^\pm \nu_l l^\pm \nu_l jj)$ and $\sigma(pp \to l^\pm \nu_l l^\mp \nu_l jj)$ at the LHC can lead to either the discovery or the exclusion of the terms in the effective Lagrangian at the permil level. This is the size of these coefficients expected on dimensional grounds. For the first time, we will be able to study the breaking of the EW symmetry at its fundamental level.

In this Introduction, we recall the relevant literature in Sec. I A, introduce the notation in Sec. I B, discuss coefficients size and higher-order terms in Sec. I C, and compare the nonlinear (chiral) Lagrangian with the linear and anomalous couplings formulations to provide a dictionary for the relevant coefficients in Sec. I D. We collect the existing limits and estimates in Sec. I E.

A. Story so far

The importance of VBS in the study of the EW symmetry breaking was recognized early on [2,7]. The unique role played by the same-sign channel was singled out in Ref. [8], and the identification of the central jet veto to distinguish the EW signal from the QCD background was first introduced in Ref. [9] where the purely leptonic "gold-plated" decay channels were also identified. In Ref. [10], the study was extended to semileptonic decay modes.

More recently, with the coming of the LHC, many different groups and authors have discussed VBS from different points of view. Of relevance for the present work, the papers in Refs. [11] and [12] have provided new insights on both the gold-plated and the semileptonic decay channel as well as the determination of resonances and the coefficients of the effective Lagrangian. In a parallel development, the extraction of bounds on anomalous triple and quartic gauge couplings from the LHC data was discussed in Ref. [13].

The parametrization of the experimental results in terms of the effective chiral Lagrangians was begun in Ref. [14] and further discussed in Refs. [4,5,15,16]. The analysis in Ref. [17] provides an estimate of the possible limits at the LHC on the leading effective Lagrangian coefficients. With respect to this work, we introduce improved selection cuts, we extend the study by including the other coefficients of the effective Lagrangian, and we update the limits for expected LHC luminosities.

For a more comprehensive review of the literature, the interested reader is referred to Ref. [18].

B. Notation

In this work, we choose to adopt the nonlinear parametrization for the EW symmetry breaking sector. This choice is particularly suitable for our purposes, since the nonlinear formulation puts the longitudinal degrees of freedom of the EW gauge bosons—dominant in the VBS processes we are interested in—in the foreground position.

The effective nonlinear Lagrangian that describes the dynamics of the Goldstone bosons associated to the $SU(2)_L \times U(1)_Y \to U(1)_{em}$ symmetry breaking pattern is organized as an expansion in powers of Goldstone bosons momenta and the ratio h/v of a light Higgs field over the EW vacuum $v = 246$ GeV; the number of possible operators is restricted by Lorentz, gauge, charge, and parity symmetry. The leading term of $O(p^2)$ can be written as

$$\mathcal{L}_0 = \frac{v^2}{4}\left[1 + 2a\frac{h}{v} + b\left(\frac{h}{v}\right)^2\right]\mathrm{Tr}[(D_\mu U)^\dagger (D^\mu U)] + \frac{1}{2}\partial_\mu h \partial^\mu h - V(h), \tag{1}$$

where a and b are coefficients parametrizing the Higgs interactions with the gauge bosons. The Goldstone bosons π^a $(a = 1, 2, 3)$ are encoded into the matrix

$$U = \exp(i\pi^a \sigma_a / v), \tag{2}$$

where σ_a are the Pauli matrices. The Goldstone matrix U has well-defined transformation properties under $SU(2)_L \times U(1)_Y$: $U \to \mathcal{G}_L U \mathcal{G}_R^\dagger$ with $\mathcal{G}_L = \exp(i\alpha^j \sigma_j/2) \in SU(2)_L$ and $\mathcal{G}_R = \exp(i\alpha_Y \sigma_3/2) \in U(1)_Y$. It constitutes the building-block for the effective Lagrangian with broken (nonlinearly realized) EW symmetry. In Eq. (1), the covariant derivative is given by

$$D_\mu U = \partial_\mu U + ig\hat{W}_\mu U - ig' U \hat{B}_\mu, \tag{3}$$

where $\hat{W}_\mu \equiv \sigma_a W_\mu^a/2$ and $\hat{B}_\mu \equiv \sigma^3 B_\mu/2$. The fields W_μ^a and B_μ are the $SU(2)_L \times U(1)_Y$ gauge fields with standard kinetic terms

$$\mathcal{L}_{\rm gauge} = -\frac{1}{2}{\rm Tr}\hat{W}_{\mu\nu}\hat{W}^{\mu\nu} - \frac{1}{2}{\rm Tr}\hat{B}_{\mu\nu}\hat{B}^{\mu\nu}, \tag{4}$$

where $\hat{W}_{\mu\nu} = \partial_\mu \hat{W}_\nu - \partial_\nu \hat{W}_\mu + ig[\hat{W}_\mu, \hat{W}_\nu]$ and $\hat{B}_{\mu\nu} = \partial_\mu \hat{B}_\nu - \partial_\nu \hat{B}_\mu$.

In Eq. (1), the quantity $V(h)$ is the Higgs boson potential with the generic structure $V(h) = \frac{1}{2}m_h^2 h^2 + d_3(m_h^2/2v)h^3 + d_4(m_h^2/8v^2)h^4$, where the parameters d_3 and d_4 are related to the triple and quartic Higgs self-interactions, respectively.

We extend the Lagrangian in Eq. (1) by adding a set of higher-dimensional operators parametrizing the $O(p^4)$ Lagrangian,

$$\begin{aligned} \mathcal{L}_1 = {} & \frac{1}{2}a_1 g g' B_{\mu\nu}{\rm Tr}(T\hat{W}^{\mu\nu}) + \frac{i}{2}a_2 g' B_{\mu\nu}{\rm Tr}(T[V^\mu, V^\nu]) \\ & + 2ia_3 g {\rm Tr}(\hat{W}_{\mu\nu}[V^\mu, V^\nu]) \\ & + a_4[{\rm Tr}(V_\mu V_\nu)]^2 + a_5[{\rm Tr}(V_\mu V^\mu)]^2, \end{aligned} \tag{5}$$

where $V_\mu = (D_\mu U)U^\dagger$ and $T \equiv U\sigma^3 U^\dagger$. The complete list of operators entering in the chiral Lagrangian at $O(p^4)$ can be found in Ref. [3]. Here, we restrict to a subset of those given by Eq. (5) because we are interested only in operators that modify triple and quartic gauge boson couplings and are relevant for VBS processes. In particular, the coefficients a_1 modifies the vertices with both two and three gauge, a_2 modifies those with three gauge bosons, a_3 modifies those with three and four gauge bosons, a_4 and a_5 modify only vertices with four gauge bosons. In principle, since the Higgs boson is a singlet, we can add a multiplicative function of h in front of all the operators of Eq. (5), a function similar to the one between squared brackets of Eq. (1) but with different coefficients, as shown in Ref. [16]. Here, we assume these corrections to be subleading and neglect them.

In the framework we have introduced, the SM corresponds to the choice $a = b = d_3 = d_4 = 1$ and $a_1 = a_2 = a_3 = a_4 = a_5 = 0$. Any departure from these values can be interpreted as the presence of new physics.

C. Coefficients size and higher-order terms

The effective field theory approach to physics beyond the SM is made into an even more powerful tool after a few assumptions on the UV physics are made. Without such, admittedly, speculative arguments, it remains a mere classification of effective operators without offering any particular physical insight.

The use of a nonlinear realization of the electroweak symmetry naturally emerges by assuming the existence of a new strongly interacting sector responsible for its breaking. The new sector can be characterized by two parameters: a coupling, g_*, and a mass scale, Λ. The latter identifies the mass of the heavy states populating the new sector. Furthermore—in the spirit of the nonlinear σ model used in Eq. (1)—it is natural to assume that the Goldstone bosons originate from the spontaneous breaking of a global symmetry of the strong sector; in this regard, the σ-model scale v is linked to the parameter of the strong sector via the relation $g_* v \approx \Lambda$. Having in mind a cutoff scale Λ of a few TeVs, the relation $g_* v \approx \Lambda$ points toward a maximally strongly coupled sector in which one expects $g_* \approx 4\pi$. In this picture, the Higgs boson emerges as a light resonance of the strong sector.

The size of the effective operators generated integrating out the heavy resonances of the strong sector can be estimated by means of the so-called naive dimensional analysis (NDA) [19]. Integrating out heavy fields at the tree level in the strong sector, the effective Lagrangian takes the general form

$$\mathcal{L}_{\rm eff} = \frac{\Lambda^4}{g_*^2}\hat{\mathcal{L}}\left[\frac{\partial_\mu}{\Lambda}, \frac{g_* h}{\Lambda}, \frac{g_* \pi^a}{\Lambda}, \frac{gA_\mu}{\Lambda}, \frac{gA_{\mu\nu}}{\Lambda^2}\right], \tag{6}$$

where A_μ $(A_{\mu\nu})$ denotes a generic gauge field (field strength) while $\hat{\mathcal{L}}$ is a dimensionless functional. For simplicity, we neglect fermionic contributions since they are not important in our setup. The most relevant information in Eq. (6) is that the Goldstone bosons and the Higgs are always accompanied by an insertion of g_* since they are directly coupled to the strong sector they belong to.

We can now analyze by power counting the effective operators, written in Eq. (5), relevant for the WW scattering process we are interested in:

(i) The effective operators $a_4[{\rm Tr}(V_\mu V_\nu)]^2$ and $a_5[{\rm Tr}(V_\mu V^\mu)]^2$ generate the quadrilinear vertex involving four Goldstone boson derivatives. Using the rules of NDA, we find the corresponding WW scattering amplitude to be proportional to $g_*^2(E/\Lambda)^4$, where E is the characteristic center-of-mass energy of the process (for the sake of simplicity, we do not distinguish here between different WW channels, since we are simply interested in an order-of-magnitude estimate of the amplitude).

(ii) The operator $a_3\mathrm{Tr}(\hat{W}_{\mu\nu}[V^\mu, V^\nu])$ generates the trilinear coupling

$$\epsilon_{kAB}(\partial_\mu W^k_\nu - \partial_\nu W^k_\mu)(\partial^\mu\pi^A\partial^\nu\pi^B - \partial^\nu\pi^A\partial^\mu\pi^B). \quad (7)$$

The corresponding WW scattering amplitude involves the s-, t-, and u-channel exchanges of the EW gauge bosons $W^{k=1,2,3}$, and from NDA, we obtain an amplitude proportional to $g^2(E/\Lambda)^4$.

(iii) The operator $a_2 B_{\mu\nu}\mathrm{Tr}(T[V^\mu, V^\nu])$ generates the trilinear coupling

$$\epsilon_{3AB}(\partial_\mu B_\nu - \partial_\nu B_\mu)(\partial^\mu\pi^A\partial^\nu\pi^B - \partial^\nu\pi^A\partial^\mu\pi^B). \quad (8)$$

The corresponding WW scattering amplitude involves the s-, t-, and u-channel exchanges of the EW gauge boson B, and from NDA, we obtain an amplitude proportional to $g'^2(E/\Lambda)^4$.

(iv) The operator $a_1 g g' B_{\mu\nu}\mathrm{Tr}(T\hat{W}^{\mu\nu})$ gives rise to an amplitude proportional to $gg'(E/\Lambda)^2$. We do not study this operator because, as discussed below, it is already severely constrained.

(v) Finally, the σ-model operator $\mathrm{Tr}[(D_\mu U)^\dagger(D^\mu U)]$ generates the trilinear structures

$$\epsilon_{kAB}W^k_\mu[(\partial^\mu\pi^A)\pi^B - (\partial^\mu\pi^B)\pi^A] \quad \text{and}$$
$$\epsilon_{3AB}B_\mu[(\partial^\mu\pi^A)\pi^B - (\partial^\mu\pi^B)\pi^A]. \quad (9)$$

By combining these vertices with the trilinear interactions extracted before from $a_3\mathrm{Tr}(\hat{W}_{\mu\nu}\times[V^\mu, V^\nu])$ and $a_2 B_{\mu\nu}\mathrm{Tr}(T[V^\mu, V^\nu])$, we find an amplitude proportional to, respectively, $g^2(E/\Lambda)^2$ and $g'^2(E/\Lambda)^2$.

Notice that the energy dependence of these amplitudes—obtained here by dimensional analysis—will be confirmed by means of a direct computation in Sec. II D.

We can now compare the amplitude proportional to $a_{4,5}$ against that proportional to a_2. Both these amplitudes grow with E^4; however, the contribution coming from the operators $a_4[\mathrm{Tr}(V_\mu V_\nu)]^2$ and $a_5[\mathrm{Tr}(V_\mu V^\mu)]^2$ is parametrically enhanced since it is proportional to g_*^2. Similarly, we can compare the same amplitude against that proportional to a_3. The former dominates if the condition $g_*(E/\Lambda) > g$ is satisfied. Since $g_* v \approx \Lambda$, it implies $E > gv$, a condition easily satisfied at typical LHC energies.

It therefore seems natural to expect that in the presence of a genuinely strongly coupled new sector the most relevant contribution to the WW scattering arises from the pure Goldstone operators $a_4[\mathrm{Tr}(V_\mu V_\nu)]^2$ and $a_5[\mathrm{Tr}(V_\mu V^\mu)]^2$. For this reason, in Sec. II, we will focus our Monte Carlo analysis on the two coefficients a_4 and a_5, setting $a_2 = a_3 = 0$.

Finally, notice that the same NDA argument can be used in order to estimate the contribution of $O(p^6)$ (or higher) operators. For definiteness, let us consider the $O(p^6)$ operator $\epsilon_{ABC}(W^A)^\nu_\mu(W^B)_{\nu\rho}(W^C)^{\rho\mu}$. It generates the quadrilinear vertex

$$\epsilon_{ABC}\epsilon_{AB'C'}(\partial_\mu W^{B,\nu} - \partial^\nu W^B_\mu)(\partial_\nu W^C_\rho - \partial_\rho W^C_\nu)W^{B',\rho}W^{C',\mu}, \quad (10)$$

which contributes to the WW (transverse) scattering according to $g^2(g^2/g_*^2)(E/\Lambda)^2$.[1] As evident from the previous discussion, the maximally strongly coupled limit $g_* \approx 4\pi$ suppresses this contribution that in principle could interfere with the perturbative expansion.

D. Mapping to other formulations

It is useful to map the nonlinear formalism into other popular parametrizations—thus providing a dictionary through which to translate all the available bounds. In the following, we briefly discuss the relations with i) the phenomenological Lagrangian commonly used to parametrize triple and quartic anomalous gauge boson couplings and ii) the higher-dimensional effective Lagrangian obtained by imposing the additional assumption that the Higgs field h is part of a $SU(2)_L$ doublet that breaks the EW symmetry.

1. Anomalous triple and quartic gauge couplings

Traditionally, bounds on triple gauge boson couplings (TGCs) have been expressed in terms of anomalous coefficients [20], according to the phenomenological Lagrangian

$$\mathcal{L}_{\mathrm{TGC}} = ie\left[g_1^\gamma A_\mu(W^-_\nu W^{+\mu\nu} - W^+_\nu W^{-\mu\nu}) + \kappa^\gamma W^-_\mu W^+_\nu A^{\mu\nu} + \frac{\lambda^\gamma}{m_W^2}W^{-\nu}_\mu W^+_{\nu\rho}A^{\rho\mu}\right] + \frac{iec_W}{s_W}\left[g_1^Z Z_\mu(W^-_\nu W^{+\mu\nu} - W^+_\nu W^{-\mu\nu}) + \kappa^Z W^-_\mu W^+_\nu Z^{\mu\nu} + \frac{\lambda^Z}{m_W^2}W^{-\nu}_\mu W^+_{\nu\rho}Z^{\rho\mu}\right], \quad (11)$$

where $W^\pm_{\mu\nu} \equiv \partial_\mu W^\pm_\nu - \partial_\nu W^\pm_\mu$, $V_{\mu\nu} \equiv \partial_\mu V_\nu - \partial_\nu V_\mu$, with $V = A, Z$. The SM corresponds to $g_1^{\gamma,Z} = \kappa^{\gamma,Z} = 1$, $\lambda^{\gamma,Z} = 0$.

[1] A further loop suppression $g_*/(4\pi)^2$ is expected, since this operator cannot be generated by integrating out at the tree level any resonance with spin less than 2. However, since we have in mind the limit $g_* \approx 4\pi$, the presence of this extra factor does not change our estimate.

In our case, κ_Z, κ_γ, and g_1^Z (g_1^γ is fixed to be 1 by gauge invariance) are modified by the presence of the operators in Eq. (5). By inspection, we can identify the following identities:

$$\begin{aligned}\Delta g_1^Z &= \frac{g'^2}{c_W^2 - s_W^2} a_1 + \frac{2g^2}{c_W^2} a_3,\\ \Delta\kappa^\gamma &= g^2(a_2 - a_1) + 2g^2 a_3,\\ \Delta\kappa^Z &= \frac{g'^2}{c_W^2 - s_W^2} a_1 - g'^2(a_2 - a_1) + 2g^2 a_3.\end{aligned} \tag{12}$$

Furthermore, it follows that $\Delta\kappa^Z = \Delta g_1^Z - (g'^2/g^2)\Delta\kappa^\gamma$. For illustrative purposes, we can take $a_1 = 0$, as suggested by the stringent fit of LEP data of Ref. [21]. In this case, the previous relations simplify to

$$\Delta g_1^Z = \frac{2g^2}{c_W^2} a_3, \qquad \Delta\kappa^\gamma - \Delta\kappa^Z = (g^2 + g'^2)a_2. \tag{13}$$

As far as the anomalous quartic gauge couplings (QGC) are concerned, they are usually parametrized as

$$\begin{aligned}\mathcal{L}_{\mathrm{QGC}} = e^2 g_{WWVV}[g_1^{VV} V^\mu V^\nu W_\mu^- W_\nu^+ - g_2^{VV} V^\mu V_\mu W^{-\nu} W_\nu^+]\\ + \frac{e^2 c_W}{s_W}[g_1^{\gamma Z} A^\mu Z^\nu (W_\mu^- W_\nu^+ + W_\mu^+ W_\nu^-) - 2g_2^{\gamma Z} A^\mu Z_\mu W^{-\nu} W_\nu^+]\\ + \frac{e^2}{2s_W^2}[g_1^{WW} W^{-\mu} W^{+\nu} W_\mu^- W_\nu^+ - g_2^{WW}(W^{-\mu} W_\mu^+)^2] + \frac{e^2}{4s_W^2 c_W^4} h^{ZZ}(Z_\mu Z^\mu)^2,\end{aligned} \tag{14}$$

with $g_{WW\gamma\gamma} = 1$, $g_{WWZZ} = c_W^2/s_W^2$. The SM corresponds to $g_{1/2}^{VV'} = 1$, $h^{ZZ} = 0$. The effective operators of Eq. (5) produce the following corrections:

$$\Delta g_1^{\gamma Z} = \Delta g_2^{\gamma Z} = \frac{g^2}{c_W^2} a_3, \qquad \Delta g_2^{ZZ} = 2\Delta g_1^{\gamma Z} - \frac{g^2}{c_W^4} a_5, \tag{15}$$

$$\Delta g_1^{ZZ} = 2\Delta g_1^{\gamma Z} + \frac{g^2}{c_W^4} a_4, \qquad \Delta g_1^{WW} = 2c_W^2 \Delta g_1^{\gamma Z} + g^2 a_4, \tag{16}$$

$$h^{ZZ} = g^2(a_4 + a_5), \qquad \Delta g_2^{WW} = 2c_W^2 \Delta g_1^{\gamma Z} - g^2(a_4 + 2a_5). \tag{17}$$

2. Comparison with the linear realization

At dimension 6, the bosonic operators relevant for our discussion are [22]

$$\begin{aligned}&\mathcal{O}_{WB} = \frac{g\kappa_{WB}}{4m_W^2} B^{\mu\nu} W_{\mu\nu}^k H^\dagger \sigma^k H, \qquad \mathcal{O}_{3W} = \frac{g\kappa_{3W}}{6m_W^2} \epsilon^{ijk} W_{\mu\nu}^i W_\rho^{j\nu} W^{k\rho\mu}, \qquad \mathcal{O}_H = \frac{\kappa_H}{v^2} \partial^\mu (H^\dagger H)\partial_\mu (H^\dagger H),\\ &\mathcal{O}_{HW} = \frac{ig\kappa_{HW}}{m_W^2}(D^\mu H)^\dagger \sigma^k (D^\nu H) W_{\mu\nu}^k, \qquad \mathcal{O}_W = \frac{ig\kappa_W}{2m_W^2} H^\dagger \sigma^k \overleftrightarrow{D}_\mu H (D_\nu W^{k\mu\nu}), \qquad \mathcal{O}_{WW} = \frac{g^2\kappa_{WW}}{4m_W^2}(H^\dagger H) W_{\mu\nu}^k W^{k\mu\nu},\\ &\mathcal{O}_{HB} = \frac{ig'\kappa_{HB}}{m_W^2}(D_\mu H)^\dagger (D_\nu H) B^{\mu\nu}, \qquad \mathcal{O}_B = \frac{ig'\kappa_B}{2m_W^2} H^\dagger \overleftrightarrow{D}_\mu H (\partial_\nu B^{\mu\nu}), \qquad \mathcal{O}_{BB} = \frac{g'^2\kappa_{BB}}{4m_W^2}(H^\dagger H) B_{\mu\nu} B^{\mu\nu},\\ &\mathcal{O}_{2W} = \frac{g^2\kappa_{2W}}{16m_W^2}(D_\rho W_{\mu\nu}^k)^2, \qquad \mathcal{O}_{2B} = \frac{g'^2\kappa_{2B}}{16m_W^2}(D_\rho B_{\mu\nu})^2,\end{aligned} \tag{18}$$

with $H^\dagger \overleftrightarrow{D}_\mu H = H^\dagger (D_\mu H) - (D_\mu H)^\dagger H$. H is the Higgs doublet of the SM with hypercharge $Y_H = 1/2$. The operators $\mathcal{O}_{H,WW,BB}$ in the last column affect only Higgs physics, while the remaining ones affect the electroweak precision observables. Three operators $\mathcal{O}_{3W}$, $\mathcal{O}_{WW}$, and $\mathcal{O}_W$ enter in WW vector boson scattering.

Notice that there is a redundancy in this list, since it is possible to remove some of these operators using the equation of motion of the gauge fields and the operator identities $\mathcal{O}_{HB} = \mathcal{O}_B - \mathcal{O}_{WB} - \mathcal{O}_{BB}$ and $\mathcal{O}_{HW} = \mathcal{O}_W - \mathcal{O}_{WB} - \mathcal{O}_{WW}$.[2]

[2]In Ref. [23] [using the notation of Eq. (18)], the subset $\{\mathcal{O}_H, \mathcal{O}_{3W}, \mathcal{O}_{HW}, \mathcal{O}_{HB}, \mathcal{O}_{WW}, \mathcal{O}_{BB}\}$ was considered.

For instance, in the strongly interacting light Higgs basis used in Ref. [24], the operators $\mathcal{O}_{2W,2B,WB,WW}$ are dropped,[3] while in the so-called Warsaw basis [25], the operators $\mathcal{O}_{2W,2B,W,B,HW,HB}$ are dropped. By comparing the anomalous TGCs, we find

$$\Delta g_1^Z = g^2\left(\frac{s_W^2}{c_W^2 - s_W^2}a_1 + \frac{2a_3}{c_W^2}\right) = \kappa_W + \kappa_{HW},$$
$$\Delta\kappa^\gamma = g^2(a_2 - a_1 + 2a_3) = -\kappa_{WB} + \kappa_{HW} + \kappa_{HB}. \tag{20}$$

There are 18 operators of dimension 8, but only two,

$$\mathcal{O}_{S,0} = \frac{f_{S,0}}{\Lambda^4}[(D_\mu H)^\dagger D_\nu H][(D^\mu H)^\dagger D^\nu H],$$
$$\mathcal{O}_{S,1} = \frac{f_{S,1}}{\Lambda^4}[(D_\mu H)^\dagger D^\mu H][(D^\nu H)^\dagger D_\nu H], \tag{21}$$

are relevant for us. The other 16 operators of dimension 8—five of which enter WW scattering—have derivative terms in the vector bosons in addition to those with the Higgs field and would have to be matched to higher-order terms in the chiral Lagrangian. For the WW channel we are interested in, we find [23]

$$a_4 = \frac{f_{S,0}}{\Lambda^4}\frac{v^4}{8}, \quad \text{and} \quad a_4 + 2a_5 = \frac{f_{S,1}}{\Lambda^4}\frac{v^4}{8}. \tag{22}$$

E. Current and estimated bounds

Current bounds on the coefficients of the operators in Eq. (5) come from EW precision measurements performed at LEP-I and LEP-II and from data collected at LHC run 1. Estimated bounds are meant to be for LHC run 2.

1. Electroweak precision tests

The coefficient a_1 is strongly constrained by LEP-I and LEP-II data because it contributes at tree level to the S parameter

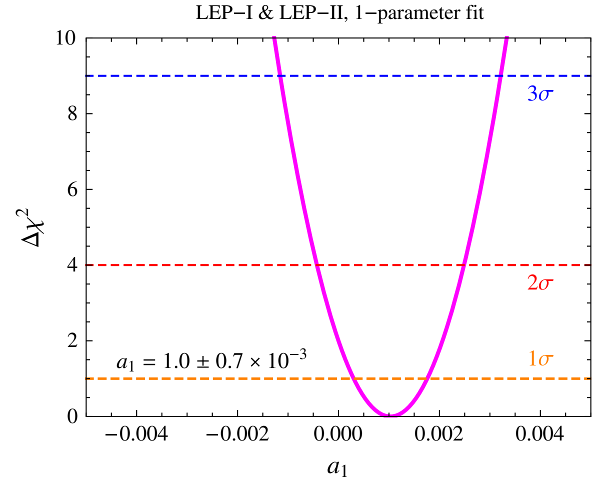

FIG. 1. $\Delta\chi^2$ plot for the limit on the coefficient a_1 from LEP I and II precision tests.

$$\Delta S = -16\pi a_1. \tag{23}$$

In Fig. 1 a simple fit of LEP data [21] performed including the correction in Eq. (23) shows that

$$a_1 = (1.0 \pm 0.7) \times 10^{-3}. \tag{24}$$

On the other hand, the other coefficients a_2, a_3, a_4, and a_5 contribute to the S, T, U parameters only at at one loop. In particular, the one-loop contributions of a_4 and a_5 to EW precision measurements lead to the following (rather weak) bounds on these coefficients at 90% C.L. [16]:

$$-0.094 < a_4 < 0.10 \quad \text{and} \quad -0.23 < a_5 < 0.26. \tag{25}$$

The combined LEP bounds on TGCs [26] are

$$-0.054 < \Delta g_1^Z < 0.021 \qquad -0.074 < \Delta\kappa_Z < 0.051$$
$$-0.099 < \Delta\kappa_\gamma < 0.066 \qquad (95\%\ \text{C.L.}). \tag{26}$$

By means of the relations in Eq. (13), we can translate the above bounds into limits on the coefficients a_2 and a_3,

$$-0.27 < a_2 < 0.25 \quad \text{and} \quad -0.05 < a_3 < 0.02, \tag{27}$$

which are in agreement with the ones found in Ref. [16].

2. LHC run 1 and run 2

New bounds on TGCs have been obtained at run 1 of the LHC [27,28]:

$$-0.047 < \Delta g_1^Z < 0.022 \qquad -0.043 < \Delta\kappa_Z < 0.033$$
$$-0.13 < \Delta\kappa_\gamma < 0.095 \qquad (95\%\ \text{C.L.}). \tag{28}$$

By combining the best limits in Eqs. (26) and (28), we have that

$$-0.24 < a_2 < 0.20 \quad \text{and} \quad -0.04 < a_3 < 0.02. \tag{29}$$

[3]At first glance, there seems to be an inconsistency between different bases since in the Warsaw basis one is left with fewer deformations in the bosonic sector. The point is that the equivalence between the two bases is realized including—in addition to the effective operators made of bosons listed before—the effective operators made out of fermions. This point can be understood by looking at the equations of motion of the gauge fields, i.e.,

$$\frac{1}{g^2}D_\nu W^i_{\mu\nu} = \frac{1}{2}H^\dagger\sigma^i \overleftrightarrow{D}_\mu H + \frac{1}{2}\sum_f \bar{f}\sigma^i\bar{\sigma}_\mu f, \tag{19}$$

where the mapping between the two sets of operators is manifest. From a phenomenological perspective, this implies that a comprehensive analysis of dimension-6 operators must include experimental bounds both on TGCs (measured at LEP-II and constraining the effective operators made of bosons) and Z/W couplings to fermions (measured at LEP-I and constraining the effective operators made of fermions).

Current experimental limits on a_4 and a_5 based on LHC run 1 are still rather weak and comparable to those in Eq. (25) coming from EW precision measurements. ATLAS and CMS find [29]

$$-0.14 < a_4 < 0.16 \quad \text{and} \quad -0.23 < a_5 < 0.24 \tag{30}$$

at the 95% C.L. and with a luminosity of 20.3 fb^{-1} (c.m. energy of 8 TeV). These bounds are obtained by studying the double charged channel (after unitarization by means of the K-matrix method).

The estimated bound on a_4 at the LHC run 2 presented in Ref. [30] is obtained at 95% C.L. and for a luminosity of 300 fb^{-1} (c.m. energy of 14 TeV):

$$a_4 \leq 0.066. \tag{31}$$

This limit is rather weak because only the opposite-sign channel is considered and the selection cuts appear not to be optimized.

The best existing estimated limit is obtained in Ref. [17] where they combine same- and opposite-sign channels. They find

$$-22 < \frac{f_0}{\Lambda^4}(\mathrm{TeV}^{-4}) < 24 \quad \text{and}$$
$$-25 < \frac{f_1}{\Lambda^4}(\mathrm{TeV}^{-4}) < 25 \tag{32}$$

at the 99% C.L. and for a luminosity of 100 fb^{-1} (c.m. energy of 14 TeV). These bounds are equivalent by means of Eq. (22) to

$$-0.01 < a_4 < 0.01 \quad \text{and} \quad -0.01 < a_5 < 0.01. \tag{33}$$

Recent data on the Higgs boson decays indicate a value for the Higgs coupling to the gauge bosons very close to the SM value, namely [31],

$$a = 1.03 \pm 0.06. \tag{34}$$

No dramatic improvement on this limit is expected from future LHC runs due to systematic errors [32].

3. *Analyticity and causality*

The causal and analytic structure of the amplitudes leads to theoretical bounds on the possible values the two coefficients a_4 and a_5 can assume [15,33]. The most stringent of these comes from the requirement that the underlying theory respects causality,

$$a_4(\mu) \geq \frac{1}{12}\frac{1}{(4\pi)^2}\log\frac{\Lambda^2}{\mu^2} \quad \text{and}$$
$$a_4(\mu) + a_5(\mu) \geq \frac{1}{8}\frac{1}{(4\pi)^2}\log\frac{\Lambda^2}{\mu^2}, \tag{35}$$

where Λ represents the cutoff of the effective theory and $\mu < \Lambda$ the scale at which the amplitude is evaluated. For most practical proposes, we can neglect the logarithms and take

$$a_4 > 0 \quad \text{and} \quad a_4 + a_5 > 0 \tag{36}$$

as our causality bounds. A violation of the above constraints implies a breakdown of the effective theory expansion caused by the presence of low-lying resonances.

II. METHODS

In Sec. II A, we present some details about the Monte Carlo simulation we have implemented in order to generate the VBS processes we are interested in. In Sec. II B, we describe the selection cuts we have employed. The statistical framework and the estimation of the effects of systematic errors are presented in Sec. II C. Finally, in Sec. II D, we discuss the violation of unitarity that can potentially arise and explain the unitarization procedure we have applied.

A. Monte Carlo simulation

We have modeled the effective Lagrangian consisting of the sum of the terms in Eqs. (1), (4), and (5) by means of FeynRules [34] v2.0.28 in order to create the Universal FeynRules output module that is used in MadGraph5 [35] v2.2.3 to simulate signal and background events related to the VBS processes we are interested in.

Pure EW same-sign (SS) WW events in $pp \to W^\pm W^\pm jj \to l^\pm \nu_l l^\pm \nu_l jj$ and EW opposite-sign (OS) WW events in $pp \to W^\pm W^\mp jj \to l^\pm \nu_l l^\mp \nu_l jj$ are $O(\alpha_W^6)$. Mixed QCD/EW SS and OS WW events are $O(\alpha_W^4 \alpha_s^2)$.

The relevant diagrams for probing the symmetry breaking dynamics must contain direct interactions of longitudinal W bosons. They are only a small fraction of the whole set in pure EW events—which are dominated by diagrams in which the W bosons are radiated from the incoming quarks and do not interact or interact but have predominantly a transverse polarization. Mixed QCD/EW events—in which the vector bosons are produced from strongly scattered quarks—only contain diagrams in which the W bosons do not interact. These two processes constitute the main irreducible background for our analysis.

Events in which the final leptons do not come from the s-channel decay of the gauge bosons should also in principle be included, but we verified that they give a small contribution (their contribution to the total cross section is 7% before cuts, and it reduces to 1.5% after the application of central jet veto cut) and can be neglected in the Monte Carlo simulation—where their inclusion would otherwise imply a substantial increase of CPU time.

Other background processes that contribute to SS and OS WW channels are the following:

(i) $Z+$jets: Events from this process can easily enter the OS channel and even the SS channel if the sign of one lepton is misidentified.

(ii) $t\bar{t}$: The same considerations apply as for $Z+$jets, but this kind of events are expected to be harder to suppress due to the higher probability of having more energetic jet and lepton pairs with large angular separation (and therefore higher invariant masses).

(iii) $WZ+$jets, $t\bar{t}W$, $t\bar{t}Z$, and $t\bar{t}H$: Events from these processes can originate high-energy jets together with two or more charged leptons, which can even enter the SS leptons selection, in case of three or more leptons or one lepton from the $t\bar{t}$ decay and another one from the associated boson decay.

(iv) Single-lepton $+$ jet (e.g., from $W+$jets): These events can enter any of the two channels if a jet is misidentified as an additional isolated lepton.

Among the processes listed above, we have included the $WZ+$jets background in the study of the SS channel and the $t\bar{t}$ background in that of the OS channel. The other processes are highly suppressed by the selection cuts, resulting in negligible effects in the analysis. We are aware that this suppression depends on our Monte Carlo simulation which does not predict correctly the effects of lepton charge misidentification and jets reconstructed as leptons in the detector.

The simulated events have been showered using Pythia 6.4 [36] and subsequently processed through Delphes [37] in order to simulate the response of a generic LHC detector. All the settings for both Pythia and Delphes have been kept as default (i.e., leaving the default options when installing the software through the Madgraph5 interface).

The number of events from each process has been then rescaled according to the leading-order cross section and the expected integrated luminosity in each of the considered cases, to obtain an expected yield after the event selection.

B. Selection cuts

As already discussed, the pure EW production of WW pairs in association with two jets at the LHC is dominated by events that have no direct relevance for the mechanism of electroweak symmetry breaking. Typically these events come from soft collisions involving incoming partons which lead to soft accompanying parton jets in the final state and can be rejected by appropriate cuts on their rapidity. To suppress this irreducible background and select events with hard WW interactions, we apply the following selection criteria:

(i) small pseudorapidity and large transverse momentum for the W gauge bosons,

(ii) two opposite tagging jets at large pseudorapidities and relatively small transverse momentum.

Beside reducing the irreducible EW background, these cuts also suppress the mixed EW/QCD one.

Subsequently, we have to impose additional cuts in order to wean out the transversally polarized vector bosons—which accounts for more than 90% of the total produced W pairs—and select the longitudinally polarized ones. At the parton level, the production of longitudinally polarized W is characterized by the final quark which is emitted more forward than in the case of the production of transversally polarized W. Moreover, after being produced by bremsstrahlung, the W_L (mostly) conserve their polarization—as long as we stay above the on-shell production threshold.

The complete set of cuts applied in the case of SS and OS WW channels is summarized below.

1. Same-sign WW channel

We select events by applying the following set of cuts:

(i) two same-sign leptons with $p_T^{l^\pm} > 20$ GeV and $|\eta_{l^\pm}| < 2.5$,

(ii) at least two jets ($p_T^j > 25$ GeV and $|\eta_j| < 4.5$) with relative rapidity $|\Delta y_{jj}| > 2.4$,

(iii) the two highest p_T jets with an invariant mass $m_{jj} > 500$ GeV,

(iv) missing transverse energy $E_T^{\rm miss} > 25$ GeV.

This combined set of cuts has been optimized for VBS at the energy of 14 TeV, considering an integrated luminosity of 300 fb^{-1}, and is rather close to those already in use by the LHC experimental collaborations.

The cuts above only partially succeed in singling out the longitudinal W bosons, and a rather large pollution from the transversally polarized ones is still present. To improve

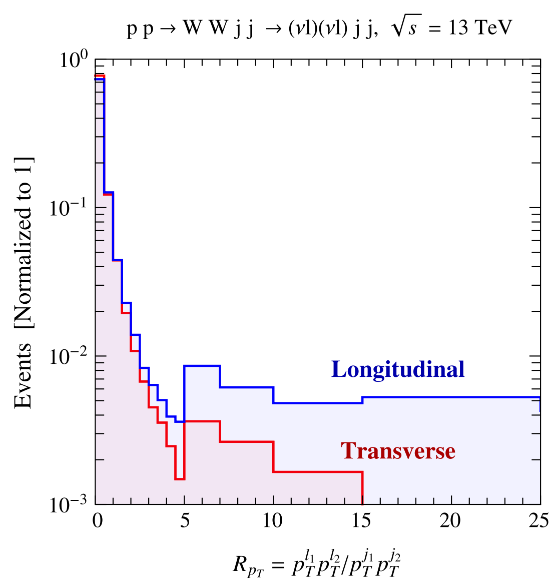

FIG. 2. Distribution of final-state events obtained generating the processes $pp \to W^\pm W^\pm jj \to (l^\pm \nu_l)(l^\pm \nu_l)jj$ at the LHC with $\sqrt{s} = 13$ TeV. We show in blue (red) the events with leptons coming from the decay of longitudinal (transverse) polarized W bosons.

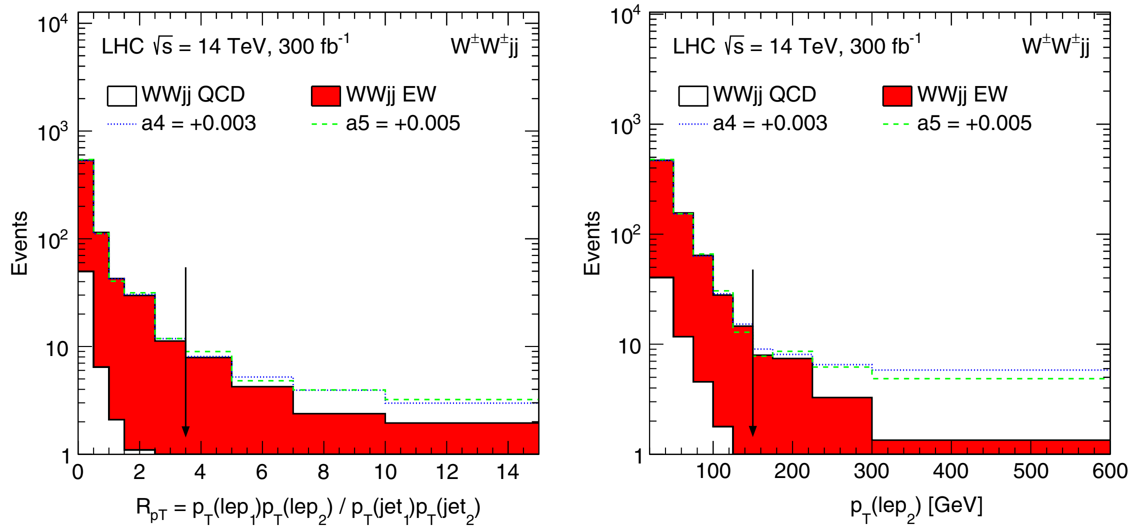

FIG. 3. Comparison of selection cuts: $R_{p_T} > 3.5$ vs $p_T^{\rm lep} > 150$ GeV. In red (white), the EW (QCD) contribution. The dashed lines mark the number of events in the presence of nonvanishing coefficients of the effective Lagrangian ($a_4 = 0.003$ and $a_5 = 0.005$).

further the selection efficiency of the longitudinal modes, we add the Warsaw cut [6], defined as follows:

$$R_{p_T} = \frac{p_T^{l_1} p_T^{l_2}}{p_T^{j_1} p_T^{j_2}} > 3.5. \tag{37}$$

The R_{p_T} variable contains the information about the momenta of the final leptons and is very effective in separating the transverse from the longitudinal modes.

The discriminating power of this cut is illustrated in the left plot of Fig. 2. The red (blue) points represent the distribution in the $[p_T^{l_1} p_T^{l_2}, p_T^{j_1} p_T^{j_2}]$ plane of $pp \to W^\pm W^\pm jj \to l^\pm \nu_l l^\pm \nu_l jj$ events at the LHC ($\sqrt{s} = 13$ TeV) containing transverse (longitudinally) polarized WW pairs. By inspection, we see that the cut $R_{p_T} > 3.5$ is very useful in discriminating longitudinal from transverse polarized W bosons. The power of this selection is even more evident from the histogram shown in the right panel of Fig 2, where the same distribution of events is plotted as a function of the ratio R_{p_T}.

In Ref. [17], the selection on the W polarization is carried out by means of a selection on the lepton momentum instead of the Warsaw cut. Figure 3 compares the two choices, and Table I shows the upper limits for the coefficients of the effective Lagrangian obtained by means of the two possible selection cuts. We find the Warsaw cut to be better in weaning out the transverse polarizations. In any case, the similarity in the selection choice is reflected in our final limits that turn out to be rather close to those of Ref. [17] for comparable energies and luminosities.

Table II shows the effect of the various selection cuts on the number of surviving events in the SS channel. Figure 4 shows the position of the cut selection for the variables Δy_{jj}, m_{jj}, and R_{p_T} for this channel.

2. Opposite-sign WW channel

The opposite-sign decay channel is less clean because of the large reducible background coming from $t\bar{t}$ pair production. For this channel, in the process $pp \to l^\pm \nu_l l^\mp \nu_l jj$, we use the following selection cuts:

TABLE I. Comparison of upper exclusion limits (at 95% and 99% C.L.) and discovery significance (at 3 and 5σ) for the effective Lagrangian coefficients a_4 and a_5, for c.m. energy $\sqrt{s} = 14$ TeV and luminosity 300 fb^{-1}, using the selection cut on R_{p_T} and p_T. Values for both coefficients obtained by only using the same-sign WW channel.

	$\sqrt{s} = 14$ TeV, 300 fb^{-1}			
	$R_{p_T} > 3.5$		$p_T^{\rm lep} > 150$ GeV	
	95% (99%)	3σ (5σ)	95% (99%)	3σ (5σ)
a_4	0.0027 (0.0034)	0.0032 (0.0041)	0.0031 (0.0038)	0.0036 (0.0047)
a_5	0.0055 (0.0068)	0.0064 (0.0084)	0.0063 (0.0078)	0.0074 (0.0097)

TABLE II. Cutflow (number of events for each process cut by cut) for the SS channel for c.m. energy $\sqrt{s} =$ 14 TeV and luminosity 300 fb^{-1}. Signal S is defined in Eq. (39) below.

	$\sqrt{s} = 14$ TeV, 300 fb^{-1}			
Cut	$WZjj$	$WWjj$ QCD	$WWjj$ EW	S ($a_4 = 0.02$)
2 SS leptons	4474	778	1343	1289
$E_T^{\rm miss} > 25$ GeV	3705	703	1225	1262
$\Delta y_{jj} > 2.4$	536	181	746	900
$m_{jj} > 500$ GeV	330	60	678	890
$R_{p_T} > 3.5$	6.5	0.5	17	747

(i) two opposite-sign leptons with $p_T^{l^\pm} > 20$ GeV and $|\eta_{l^\pm}| < 2.5$,
(ii) missing transverse energy $E_T^{\rm miss} > 25$ GeV,
(iii) the two highest p_T jets with an invariant mass $m_{jj} > 500$ GeV,
(iv) two and only two jets ($p_T^j > 25$ GeV and $|\eta_j| < 4.5$) with relative rapidity $|\Delta y_{jj}| > 2.4$,
(v) $R_{p_T} > 3.5$,
(vi) invariant transverse mass $m_T^{WW} > 800$ GeV,
(vii) angular separation between the leptons in the transverse plane $|\Delta\Phi_{ll}| > 2.25$,
(viii) b-quark veto (i.e., no jets tagged by the b-tagging algorithm implemented in Delphes).

The invariant tranverse mass in the cuts above is defined as

$$m_T^{WW} = \sqrt{\left(\sqrt{(p_T^{ll})^2 + m_{ll}^2} + \sqrt{(E_T^{\rm miss})^2 + m_{ll}^2}\right)^2 - (\vec{p}_T^{\,ll} + \vec{p}_T^{\,\rm miss})^2}, \tag{38}$$

where $\vec{p}_T^{\,\rm miss}$ is the missing transverse momentum vector, $\vec{p}_T^{\,ll}$ is the transverse momentum of the dilepton pair, and m_{ll} is its mass.

Table III shows the effect of the various selection cuts on the number of surviving events in the OS channel. Figure 5 shows the position of the cut selection for the variables $\Delta\Phi_{\ell\ell}$, Δy_{jj}, m_{jj}, $m_{\ell\ell}$, and R_{p_T} for this channel.

C. Statistical analysis

In the following, we will compute the expected discovery significance and the expected exclusion limits for the coefficients of the effective Lagrangian in Eqs. (1) and (5).

For a given set of selection cuts, we define the signal S as the enhancement in the number of $WWjj$ events—obtained for certain fixed values of the coefficients a, a_2, a_3, a_4, and a_5—over the SM prediction (obtained for $a = 1$, $a_2 = a_3 = a_4 = a_5 = 0$)

$$S = \mathcal{N}_{\rm ev}(pp \to WWjj)|_{a,a_2,a_3,a_4,a_5} - \mathcal{N}_{\rm ev}(pp \to WWjj)|_{a=1,a_2=a_3=a_4=a_5=0}. \tag{39}$$

The background B is given by the number of events predicted by the SM,

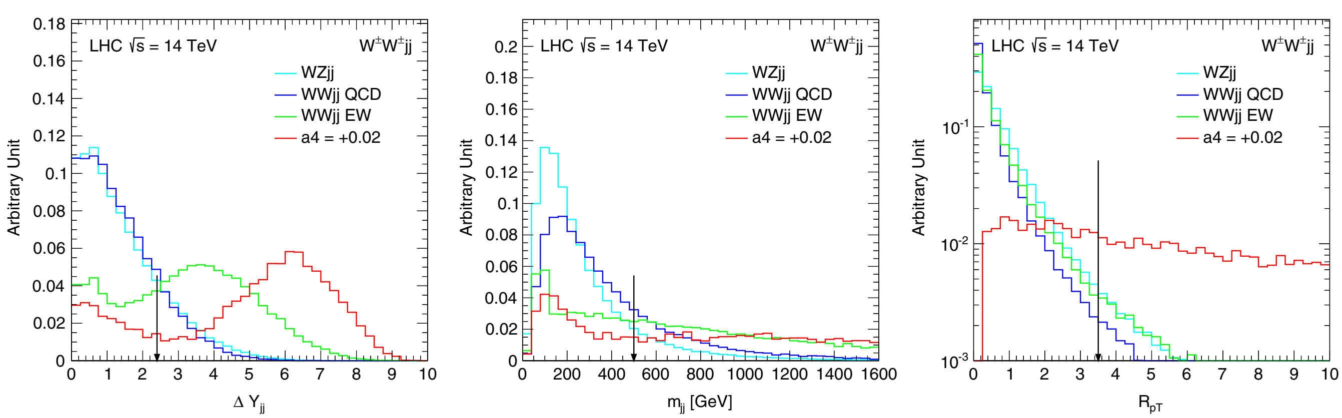

FIG. 4. Position of the cut selection for the three variables Δy_{jj}, m_{jj}, and R_{p_T} in the SS channel. Distributions are shown with no cuts except having only 2 SS leptons in the final states.

TABLE III. Cutflow (number of events for each process cut by cut) for the OS channel for c.m. energy $\sqrt{s} =$ 14 TeV and luminosity 300 fb^{-1}. Signal S is defined in Eq. (39) below.

$\sqrt{s} = 14$ TeV, 300 fb^{-1}				
Cut	$t\bar{t}$	$WWjj$ QCD	$WWjj$ EW	S ($a_5 = 0.02$)
2 OS leptons	1 975 270	68 884	3221	498
$E_T^{\mathrm{miss}} > 25$ GeV	1 791 100	61 494	2927	488
$m_{jj} > 500$ GeV	109 885	6761	1569	380
$\Delta y_{jj} > 2.4$	78 144	4543	1369	394
$R_{p_T} > 3.5$	1461	114	44	287
$m_T^{WW} > 800$ GeV	504	40	19	231
$\Delta\Phi_{\ell\ell} > 2.25$	453	34	19	231
b-tag veto	353	34	19	227
N jets < 3	21	14	11	148

$$B = \mathcal{N}_{\mathrm{ev}}(pp \to WWjj)|_{a=1,a_2=a_3=a_4=a_5=0} + \mathcal{N}_{\mathrm{ev}}(pp \to t\bar{t}/WZjj)|_{a=1,a_2=a_3=a_4=a_5=0}. \qquad (40)$$

The expected number of signal events S is compared with the number of background events B using Poisson statistics without considering any systematic uncertainty. The Poisson probability density function is generalized to noninteger event numbers through the use of the Gamma function.

1. Discovery significance and exclusion limits

For each set of values of the effective couplings, the expected discovery significance is obtained by computing the probability of observing a number of events greater than or equal to $S + B$ assuming the background-only hypothesis. This probability is then translated into a number of Gaussian standard deviations: three (five) standard deviations is considered as benchmark for an observation (discovery). On the other hand, the expected exclusion

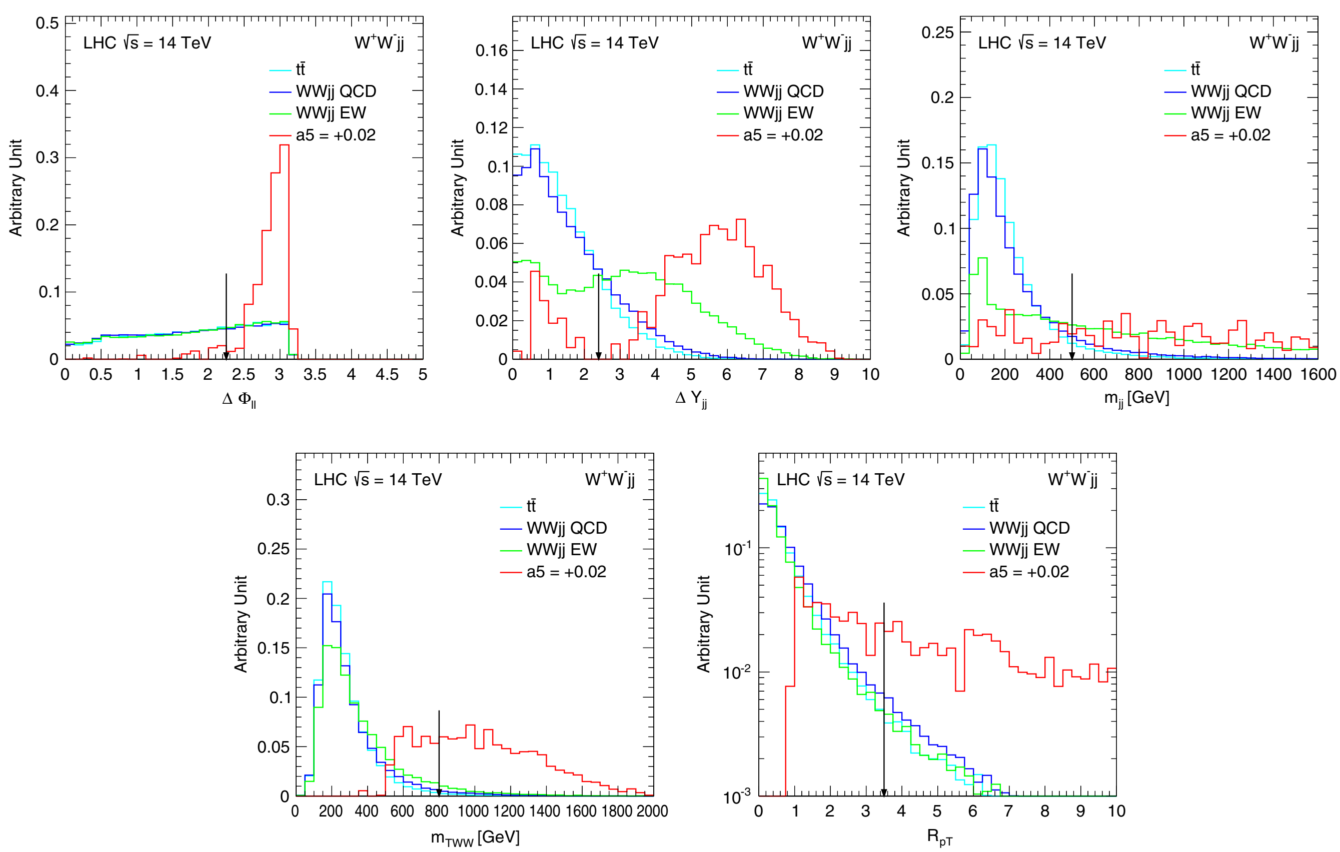

FIG. 5. Position of the cut selection for the three variables $\Delta\Phi_{\ell\ell}$, Δy_{jj}, m_{jj}, m_T^{WW}, and R_{p_T} in the OS channel. Distributions are shown with no cuts except having only 2 OS leptons in the final states.

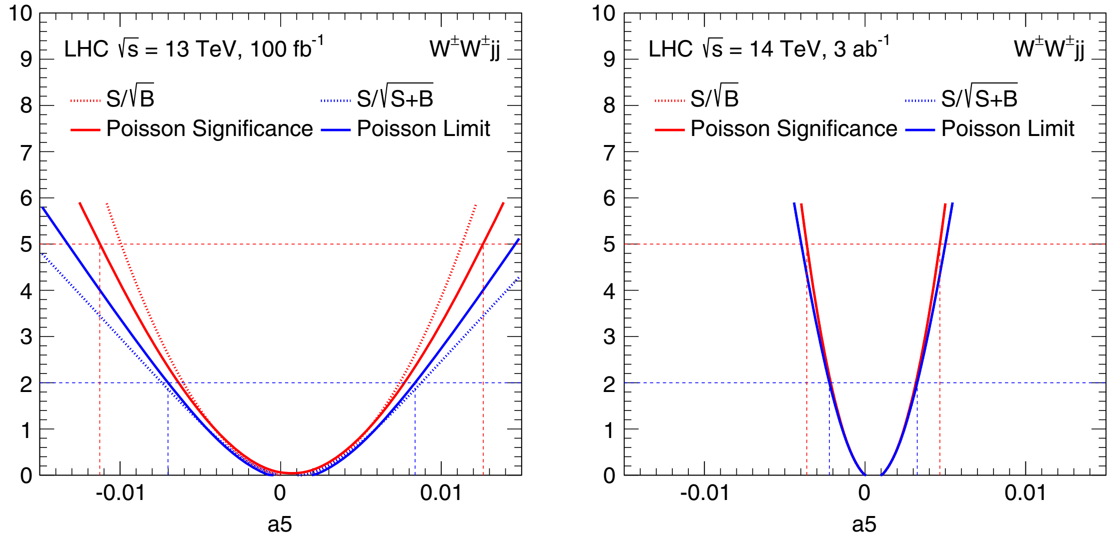

FIG. 6. $\Delta\chi^2$ plot for the coefficient a_5 using the Poisson distribution and the simplified formulas. The plot on the right shows the presence of a discrepancy at low luminosity ($\sqrt{s} = 13$ TeV, luminosity 100 fb^{-1}). The plot on the right shows that there is no discrepancy at higher luminosity ($\sqrt{s} = 14$ TeV, luminosity 3 ab^{-1}) where it is impossible to discriminate the continuous from the dashed lines.

limits are obtained by computing the probability of observing a number of events less than or equal to B assuming the signal-plus-background hypothesis. The specific choice of the parameters is considered excluded at 95% (99%) C.L. if this probability is less than or equal than 5% (1%).

Notice that, for large values of B, the Poisson distribution can be very well approximated by a Gaussian function. In this case, the significance (expressed in terms of the number of standard deviations) can be computed simply as $S/\sqrt{B}$. In the same limit, we can say that a set of parameters is excluded at 95% (99%) C.L. if the quantity $S/\sqrt{S+B} > 2$ (> 3).

The difference between using the exact Poisson distribution and the approximated formulas above can be gauged in Fig. 6 where the χ^2 test is run for the two possibilities. As one can see by inspection, while for the case at $\sqrt{s} =$ 13 TeV and luminosity 100 fb^{-1} the difference cannot be ignored, there is no difference for the higher energy and luminosity case. We employ in all cases the Poisson probability distribution.

2. Systematic uncertainties

All the results reported in the following are obtained neglecting any systematic uncertainty on the prediction for the number of signal and background events (S and B) because such uncertainties are mostly related to the experimental techniques used to extract the results. To have a feeling of the size of their effect on the results, we have included a nonzero systematic uncertainty on B and compared the limits and the significance with the case without systematics. This comparison is done considering the simplified statistics treatment described above—that is, by considering the formulas $S/\sqrt{B}$ and $S/\sqrt{S+B}$. These two expressions are generalized to the case with nonzero systematic uncertainty as $S/\sqrt{B+\delta^2\cdot B^2}$ and $S/\sqrt{S+B+\delta^2\cdot B^2}$, respectively, where δ indicate the relative systematic uncertainty on the expected number of background events B.

Table IV (and the corresponding plots in Figs. 7 and 8) shows the result of this comparison, performed considering two benchmark c.m. energy and luminosity scenarios for the two coefficients a_4 and a_5 and a relative systematic uncertainty on B of 10%. The smaller statistical error in the case of c.m. energy $\sqrt{s} = 14$ TeV and luminosity 3 ab^{-1} makes the systematic error—assumed to remain the same—more important.

As expected, the effect is rather important, especially for large values of integrated luminosity where the Gaussian error is smaller, and one should bear that in mind. Of course, an eventual reduction of such a systematic uncertainty, for instance, down at 5%, would proportionally reduce the effect, and depending on the size of this

TABLE IV. Upper limits (at 95% C.L.) for the effective Lagrangian coefficients a_4 and a_5, for two representative c.m. energies and luminosities, from the channel $W^\pm W^\pm jj$. Comparison with and without the inclusion of a systematic error of 10%.

	$\sqrt{s} = 13$ TeV, 100 fb^{-1}		$\sqrt{s} = 14$ TeV, 3 ab^{-1}	
	Without	With	Without	With
a_4	0.0043	0.0043	0.0016	0.0021
a_5	0.0088	0.0089	0.0032	0.0041

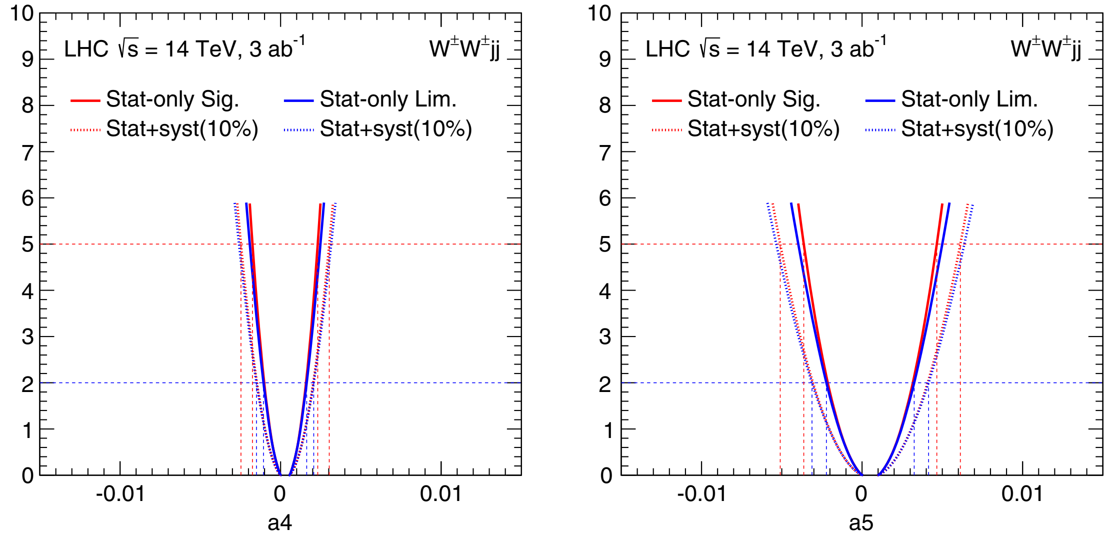

FIG. 7. $\Delta\chi^2$ plot for the coefficient a_4 (left) and a_5 (right) with and without 10% of systematic uncertainty for c.m. energy $\sqrt{s} =$ 14 TeV and luminosity 3 ab^{-1}.

uncertainty in a real experiment, selection cuts could be further tightened to minimize its impact.

D. Unitarization

For values of the coefficients a, a_2, a_3, a_4, and a_5 which are different from the SM ones, the computation of the cross section $\sigma(pp \to WWjj)$ obtained using the Lagrangian in Eqs. (1) and (5) cannot be trusted because of a possible unitarity violation that can arise at the level of some hard scattering diagrams, in particular, the ones that involve longitudinal W bosons. In this case, the cross section of the process $W_L W_L \to W_L W_L$ breaks unitarity at energies larger than the TeV (the exact violation energy depends on the specific values of the coefficients).

This breakdown in unitarity can be understood by looking at the longitudinal W bosons scattering amplitudes in the same- and opposite-sign channels—computed using the equivalence theorem in the isospin limit—which can be written in terms of isospin amplitudes $A_I(s,t)$ as

$$A(W_L^\pm W_L^\pm \to W_L^\pm W_L^\pm) = A_2 \quad \text{and}$$
$$A(W_L^\pm W_L^\mp \to W_L^\pm W_L^\mp) = \frac{1}{3}A_0 + \frac{1}{2}A_1 + \frac{1}{6}A_2. \quad (41)$$

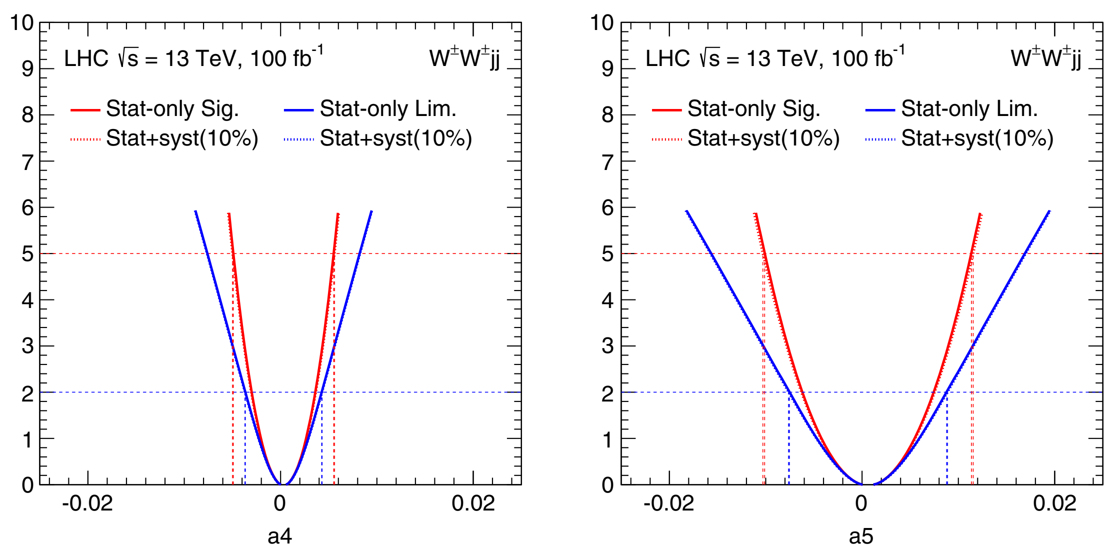

FIG. 8. $\Delta\chi^2$ plot for the coefficient a_4 (left) and a_5 (right) with and without 10% of systematic uncertainty for c.m. energy $\sqrt{s} =$ 13 TeV and luminosity 100 fb^{-1}.

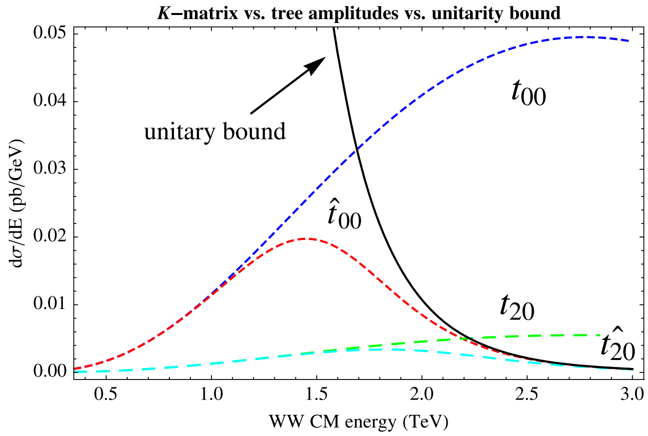

FIG. 9. Cross sections for the scattering of longitudinal W bosons as a function of the c.m. energy. In green (blue), the contribution of the partial wave t_{20} (t_{00}) for $a_4 = a_5 = 0.001$; in cyan (red), the same result after unitarization by the K matrix. The continuous black line marks the loss of unitarity for $|t_{IJ}(s)| > 1$.

The amplitudes $A_I(s,t)$ can be expanded in terms of partial waves $t_{IJ}(s)$ as

$$A_I(s,t) = 32\pi \sum_{J=0}^{\infty} (2J+1) P_J(\cos\theta) t_{IJ}(s), \tag{42}$$

where

$$t_{IJ}(s) = \frac{1}{64\pi} \int_{-1}^{1} d\cos\theta A_I(s,t) P_J(\cos\theta). \tag{43}$$

In our case, at tree level, neglecting partial waves higher than the leading $J = 0$ wave, we have

$$\begin{aligned} t_{00} = & \frac{s}{16\pi v^2}(1 - a^2 + 3g'^2 a_2 + 12 g^2 a_3) \\ & + \frac{s^2}{12\pi v^4}[11 a_5 + 7 a_4 - 2 g'^2 a_2^2 + 16 g^2 a_3^2] \end{aligned} \tag{44}$$

$$\begin{aligned} t_{20} = & -\frac{s}{32\pi v^2}(1 - a^2 - 6 g'^2 a_2 + 12 g^2 a_3) \\ & + \frac{s^2}{6\pi v^4}[a_5 + 2 a_4 - g'^2 a_2^2 - 4 g^2 a_3^2]. \end{aligned} \tag{45}$$

The isospin amplitudes $A_I(s,t)$ can then be reobtained from the partial waves computed above by means of Eq. (42). In the approximation of neglecting partial waves higher than $J = 0$, we have very simple relations:

$$\begin{aligned} & A_0(s,t) = 32\pi t_{00}, \qquad A_1(s,t) = 0 \quad \text{and} \\ & A_2(s,t) = 32\pi t_{20}. \end{aligned} \tag{46}$$

An example of such a unitarity violation ($|t_{IJ}(s)| > 1$) is shown in Fig. 9, where—for values of $a_4 = a_5 = 0.001$—it occurs around 1.5 and 2 TeV for, respectively, the isospin $I = 0$ and $I = 2$ component.

The amplitudes in Eq. (46) violate unitarity, and we interpret them as an incomplete approximation to the true amplitudes. One can deal with this problem either by cutting off the collection of events at a given value of the c.m. energy or by implementing a unitarization procedure.

As an example of the latter, let us look for unitary matrix elements that provide a nonperturbative completion. By inspection of the amplitudes, we see that the SS WW channel can only contain double-charged $I = 2$ resonances in the s channel, the first two being of spin 0 and 2. We assume that these states are sufficiently heavy to be outside the energy reach of the LHC. By extension, we assume that no resonance is present within the LHC energy range also in the opposite-sign WW channel. Therefore, the most appropriated unitarization procedure for our case in which we do not expect resonances is the K-matrix prescription [38]. The K-matrix ansatz consists in using the optical theorem

$$\mathrm{Im} t_{IJ}(s) = |t_{IJ}(s)|^2 \tag{47}$$

in order to impose the following condition on the unitarized partial wave $\hat{t}_{IJ}(s)$:

$$\mathrm{Im} \frac{1}{\hat{t}_{IJ}(s)} = -1. \tag{48}$$

The K-matrix unitarized partial wave is then defined to be

$$\hat{t}_{IJ}(s) = \frac{t_{IJ}(s)}{1 - i t_{IJ}(s)}, \tag{49}$$

TABLE V. Comparison of upper exclusion limits (at 95% and 99% C.L.) and discovery significance (at 3 and 5σ) for the effective Lagrangian coefficients a_4 and a_5, for c.m. energy $\sqrt{s} = 14$ TeV and luminosity 300 fb^{-1}, using the K-matrix and the sharp cutoff unitarization procedures. Values are obtained by using the SS WW channel.

	$\sqrt{s} = 14$ TeV, 300 fb^{-1}			
	K matrix		Sharp cutoff ($E_{WW} < 1.25$ TeV)	
	95% (99%)	3σ (5σ)	95% (99%)	3σ (5σ)
a_4	0.0028 (0.0038)	0.0035 (0.0053)	0.0027 (0.0034)	0.0032 (0.0041)
a_5	0.0053 (0.0072)	0.0066 (0.0107)	0.0055 (0.0068)	0.0064 (0.0084)

where $t_{IJ}(s)$ is the tree-level partial wave amplitude. The quantity $\hat{t}_{IJ}(s,t)$ satisfies by construction the optical theorem and is supposed to represent a resummation of the higher-order terms of which the contributions restore unitarity. The result of this unitarization is shown in Fig. 9 and compared to the tree-level result.

If we define the rescaling factor for the SS WW events,

$$r_{++}(s,a_3,a_4,a_5) = \frac{|\hat{t}_{20}|^2}{|t_{20}|^2}, \tag{50}$$

we can use it to reweight the events that survive after having applied all the selection cuts, in order to obtain a result that satisfies the unitarity bound. This procedure is reliable if the events that survive after the selection cuts are dominated by the production of longitudinal polarized W.

The K-matrix *ansatz* and the cutoff in energy are two possible procedures to deal with the violation of unitarity. Table V shows that the two procedures (for an appropriate choice of cutoff) are substantially equivalent. Their differences quantify the dependence on the unitarization procedure of the limits and provide an estimate of the impact of higher-order operators. The actual uncertainty of the limits obtained by means of the truncated effective theory is hard to gauge and may be larger than that suggested by the numbers in Table V.

Because it is more difficult to define a rescaling for the OS channel as done above for the SS channel,

TABLE VI. Exclusion limits (at 95% and 99% C.L.) and discovery significance (at 3 and 5σ) for the effective Lagrangian coefficients a_5, a_4, a_3, a_2, and a for c.m. energy $\sqrt{s} = 13$ TeV and two benchmark luminosities for LHC run 2. Values are obtained by varying the coefficients one at the time. All limits are obtained from the $W^\pm W^\pm jj$ SS channel.

	$\sqrt{s}=13$ TeV ($W^\pm W^\pm jj$ SS channel)			
	100 fb^{-1}		300 fb^{-1}	
	95% (99%)	3σ (5σ)	95% (99%)	3σ (5σ)
a_5	+0.0084(+0.0105)	+0.0095(+0.0126)	+0.0062(+0.0077)	+0.0072(+0.0094)
	−0.007(−0.0092)	−0.0082(−0.0113)	−0.0049(−0.0063)	−0.0059(−0.008)
a_4	+0.0041(+0.0052)	+0.0047(+0.0062)	+0.003(+0.0037)	+0.0035(+0.0046)
	−0.0035(−0.0046)	−0.004(−0.0056)	−0.0024(−0.0031)	−0.0029(−0.004)
a_3	+0.097(+0.121)	+0.109(+0.143)	+0.074(+0.089)	+0.085(+0.108)
	−0.072(−0.096)	−0.085(−0.118)	−0.049(−0.065)	−0.060(−0.083)
a_2	+1.63(+2.03)	+1.84(+2.41)	+1.24(+1.5)	+1.42(+1.82)
	−1.21(−1.61)	−1.42(−1.99)	−0.82(−1.09)	−1.01(−1.4)
a	+1.52(+1.6)	+1.56(+1.68)	+1.43(+1.49)	+1.47(+1.56)
	0.17(−0.44)	−0.11(−1.57)	0.54 (0.31)	0.39(−0.07)

TABLE VII. Exclusion limits (at 95% and 99% C.L.) and discovery significance (at 3 and 5σ) for the effective Lagrangian coefficients a_5, a_4, a_3, a_2, and a for c.m. energy $\sqrt{s} = 14$ TeV and two benchmark luminosities for LHC run 3. Values are obtained by varying the coefficients one at the time. All limits are obtained from the $W^\pm W^\pm jj$ SS channel.

	$\sqrt{s}=14$ TeV ($W^\pm W^\pm jj$ SS channel)			
	300 fb^{-1}		3 ab^{-1}	
	95% (99%)	3σ (5σ)	95% (99%)	3σ (5σ)
a_5	+0.0055(+0.0068)	+0.0064(+0.0084)	+0.0032(+0.0039)	+0.0037(+0.0047)
	−0.0045(−0.0058)	−0.0054(−0.0074)	−0.0022(−0.0029)	−0.0027(−0.0036)
a_4	+0.0027(+0.0034)	+0.0032(+0.0041)	+0.0016(+0.0019)	+0.0019(+0.0023)
	−0.0022(−0.0028)	−0.0026(−0.0036)	−0.0011(−0.0014)	−0.0013(−0.0018)
a_3	+0.073(+0.089)	+0.084(+0.108)	+0.046(+0.054)	+0.052(+0.063)
	−0.050(−0.065)	−0.061(−0.084)	−0.023(−0.030)	−0.028(−0.039)
a_2	+1.14(+1.37)	+1.30(+1.64)	+0.75(+0.86)	+0.83(+0.99)
	−0.70(−0.93)	−0.86(−1.21)	−0.31(−0.42)	−0.39(−0.55)
a	+1.37(+1.43)	+1.42(+1.5)	+1.27(+1.3)	+1.29(+1.33)
	0.64 (0.47)	0.52 (0.22)	0.86 (0.81)	0.82 (0.73)

TABLE VIII. Exclusion limits (at 95% and 99% C.L.) and discovery significance (at 3 and 5σ) for the effective Lagrangian coefficients a_5, a_4, a_3, a_2, and a for c.m. energy $\sqrt{s} = 13$ TeV and two benchmark luminosities for LHC run 2. Values are obtained by varying the coefficients one at the time. All limits are obtained from the $W^{\pm}W^{\mp}jj$ OS channel.

	$\sqrt{s} = 13$ TeV ($W^{\pm}W^{\mp}jj$ OS channel)			
	100 fb^{-1}		300 fb^{-1}	
	95% (99%)	3σ (5σ)	95% (99%)	3σ (5σ)
a_5	+0.0089(+0.0114)	+0.0105(+0.0141)	+0.0064(+0.0081)	+0.0077(+0.0103)
	−0.0095(−0.012)	−0.011(−0.0147)	−0.007(−0.0087)	−0.0083(−0.0109)
a_4	+0.0141(+0.0179)	+0.0165(+0.0221)	+0.0103(+0.0129)	+0.0123(+0.0162)
	−0.014(−0.0178)	−0.0164(−0.022)	−0.0102(−0.0128)	−0.0122(−0.0161)
a_3	+0.198(+0.245)	+0.227(+0.295)	+0.152(+0.183)	+0.176(+0.224)
	−0.149(−0.195)	−0.178(−0.246)	−0.103(−0.134)	−0.127(−0.174)
a_2	+1.17(+1.48)	+1.36(+1.81)	+0.87(+1.07)	+1.03(+1.34)
	−1.07(−1.37)	−1.26(−1.70)	−0.77(−0.97)	−0.92(−1.24)
a	+1.83(+2.08)	+1.99(+2.35)	+1.58(+1.75)	+1.71(+1.97)
	−0.41(−0.65)	−0.56(−0.92)	−0.19(−0.34)	−0.30(−0.54)

and because of the additional assumptions entering the K-matrix procedure, we follow the simplest procedure and introduce a sharp cutoff in the data collection so as to make the amplitudes unitary.

The cutoff must be chosen to be less than $4\pi v$, the limit for the chiral Lagrangian expansion, and below the range in which the growth becomes too fast. We take $m_{WW} <$ 1.25 TeV for the SS channel and < 2 TeV for the OS channel. It can be shown that for these values, as in Table V, differences between the two unitarization procedures are minimal.

III. RESULTS

As discussed in Sec. II A, we have generated events in which the coefficients of the effective Lagrangians in Eqs. (1) and (5) of Sec. I B, parametrizing deviations from the SM, were allowed to vary. We consider only the coefficients a, a_2, a_3, a_4, and a_5 because the coefficient a_1 is already severely constrained by LEP data, as discussed in Sec. I E, and we assume it vanishing in our analysis. The coefficients a_4 and a_5, according to our discussion in Sec. I C, are the leading and most important ones. They should be searched first. Once they have been constrained, the simulation for the coefficients a_2, a_3, and a can be carried out after setting a_4 and a_5 equal to zero.

We report in Tables VI–IX the results in terms of exclusion limits (95 and 99% C.L.) and discovery significance (3 and 5σ)—as discussed in Sec. II C—for the benchmark luminosities of 100 and 300 fb^{-1} (at a c.m. energy of $\sqrt{s} = 13$ TeV) and 300 fb^{-1} and 3 ab^{-1} (at $\sqrt{s} = 14$ TeV). All coefficients are varied here one at the time.

As it can be seen from Tables VI–IX, the OS channel does not provide stronger limits for any of the coefficients,

TABLE IX. Exclusion limits (at 95% and 99% C.L.) and discovery significance (at 3 and 5σ) for the effective Lagrangian coefficients a_5, a_4, a_3, a_2, and a for c.m. energy $\sqrt{s} = 14$ TeV and two benchmark luminosities for LHC run 3. Values are obtained by varying the coefficients one at the time. All limits are obtained from the $W^{\pm}W^{\mp}jj$ OS channel.

	$\sqrt{s} = 14$ TeV ($W^{\pm}W^{\mp}jj$ OS channel)			
	300 fb^{-1}		3 ab^{-1}	
	95% (99%)	3σ (5σ)	95% (99%)	3σ (5σ)
a_5	+0.0061(+0.0077)	+0.0073(+0.0097)	+0.0033(+0.0041)	+0.004(+0.0052)
	−0.0062(−0.0077)	−0.0074(−0.0098)	−0.0034(−0.0042)	−0.0041(−0.0052)
a_4	+0.0084(+0.0107)	+0.0102(+0.0136)	+0.0043(+0.0055)	+0.0053(+0.007)
	−0.0097(−0.012)	−0.0115(−0.0149)	−0.0056(−0.0068)	−0.0066(−0.0083)
a_3	+0.134(+0.165)	+0.158(+0.205)	+0.077(+0.094)	+0.091(+0.114)
	−0.115(−0.146)	−0.140(−0.187)	−0.059(−0.075)	−0.072(−0.096)
a_2	+0.75(+0.93)	+0.89(+1.17)	+0.42(+0.52)	+0.50(+0.64)
	−0.71(−0.89)	−0.85(−1.13)	−0.38(−0.47)	−0.45(−0.59)
a	+1.56(+1.67)	+1.64(+1.81)	+1.36(+1.41)	+1.40(+1.49)
	−0.50(−1.35)	−1.15(−2.74)	0.55 (0.31)	0.36(−0.06)

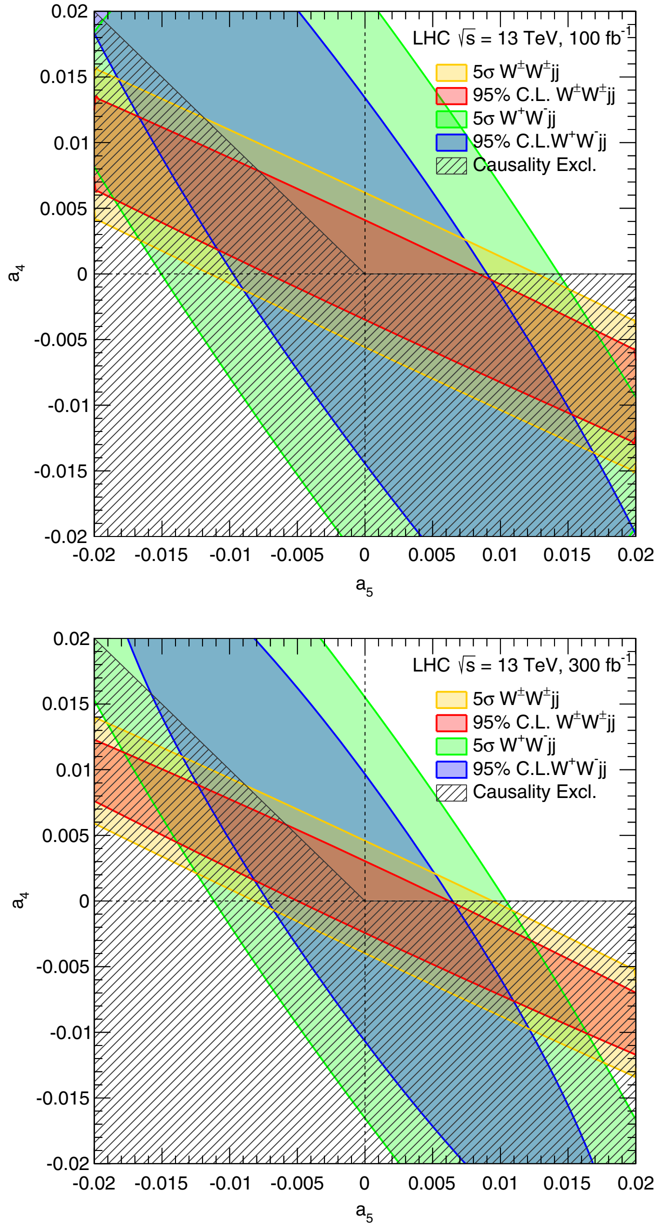

FIG. 10. Exclusion limits (at 95% C.L.) and discovery significance (5σ) for the effective Lagrangian coefficients a_4 and a_5 at c.m. energy $\sqrt{s} = 13$ TeV from the same-sign (in yellow/orange) and opposite-sign (in light green/blue) channels. The area where causality would be violated is hatched in gray.

and the SS channel is sufficient by itself in setting the most stringent constraints as long as the coefficients are varied one at the time.

Figures 10 and 11 show the exclusion limits (95% C.L.) and discovery significance (5σ) for the coefficients a_4 and a_5 obtained from the SS and OS *WW* channels for, respectively, c.m. energy $\sqrt{s} = 13$ and 14 TeV and the benchmark luminosities. The coefficients a_4 and a_5 are now varied simultaneously, and both channels contribute to the limits if the causality constraints in Eq. (36) are not assumed.

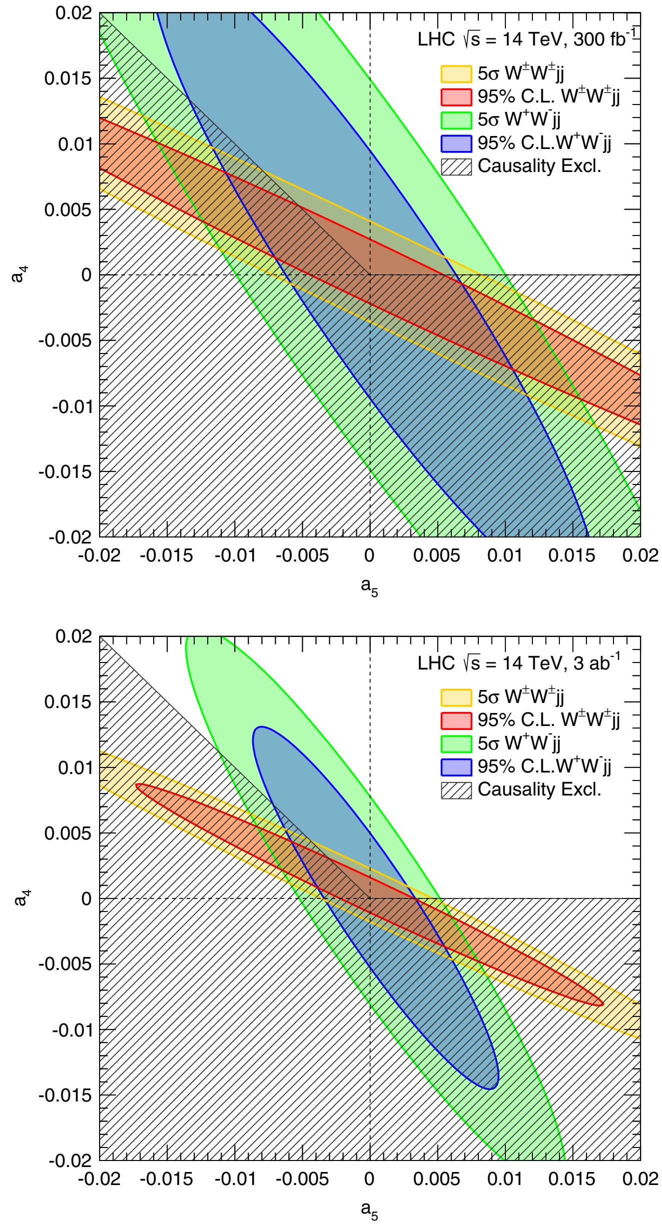

FIG. 11. Same as in Fig. 10 for c.m. energy $\sqrt{s} = 14$ TeV.

IV. DISCUSSION

While the presence of resonances is the most dramatic signal for a strongly interacting sector, they may be too heavy or broad to be clearly seen at the LHC. The discovery of a nonvanishing coefficient of the effective Lagrangian in Eq. (5), introduced in Sec. I B, is a more systematic way to search for the presence of the strongly interacting sector behind the breaking of the EW symmetry. In addition, exclusion limits provide an indirect indication about the energy scale of the masses of those resonances that are expected from such new interactions.

The identification of the most appropriated selection cuts is crucial, but it is now well understood that—in addition to the central jet veto necessary to remove the QCD background—the control of the large EW background can be achieved by means of a selection on the transverse momenta of the jets and final leptons.

We have shown that a significant improvement in both discovery significance and exclusion limits for the chiral effective Lagrangian coefficients a_4 and a_5 can be expected from the current and the next run of the LHC. Already at c.m. energy $\sqrt{s} = 13$ TeV and a luminosity of 100 fb^{-1}, the limits will reach the permil precision, thus coming within range of the values expected by purely dimensional analysis. The results for a_4 and a_5 varied one at the time can be obtained by studying the SS $WW \to WW$ channel alone. The OS channel as well as the SS channel contribute to the limits when the coefficients a_4 and a_5 are varied simultaneously if the causality constraints are not assumed.

The determination of the coefficient a_3 within VBS—the best limits for which come at the moment from precision measurements—will become competitive already at LHC run 2 when a luminosity of 300 fb^{-1} will be available. The coefficient a_2 gives rise to smaller deviations in VBS and is determined with less precision; its constraints will be competitive with those from TGC data only when higher luminosities become available.

Finally, the coefficient a—controlling the coupling of the Higgs to the vector bosons in Eq. (1) in Sec. I B—remains best determined in the decay processes of the Higgs boson. Only at future LHC runs will a comparable limit be available from VBS.

While VBS remains our best laboratory to study EW symmetry breaking, the presence of systematic errors hard to reduce and even estimate will eventually limit the final precision of the measurements that can be achieved at the LHC. The same is true for the study of the Higgs boson decays and the complementary determination of the coefficient a, as defined in Eq. (1) in Sec. I B.

ACKNOWLEDGMENTS

We thank O. Éboli and F. Riva for discussions. M. F. is associated with SISSA. The work of A. T. is supported by FAPESP, the São Paulo Research Foundation under Grants No. 2011/11973-4 and No. 2013/02404-1. The work of M. P. and A. U. is supported by the ERC Advanced Grant No. 267985, “Electroweak Symmetry Breaking, Flavour and Dark Matter: One Solution for Three Mysteries.”

[1] G. Aad *et al.* (ATLAS Collaboration), Phys. Lett. B **716**, 1 (2012); S. Chatrchyan *et al.* (CMS Collaboration), Phys. Lett. B **716**, 30 (2012).

[2] M. S. Chanowitz and M. K. Gaillard, Nucl. Phys. **B261**, 379 (1985).

[3] T. Appelquist and C. W. Bernard, Phys. Rev. D **22**, 200 (1980); A. C. Longhitano, Phys. Rev. D **22**, 1166 (1980); T. Appelquist and G. H. Wu, Phys. Rev. D **48**, 3235 (1993).

[4] D. Espriu and B. Yencho, Phys. Rev. D **87**, 055017 (2013); D. Espriu and F. Mescia, Phys. Rev. D **90**, 015035 (2014).

[5] R. L. Delgado, A. Dobado, and F. J. Llanes-Estrada, J. Phys. G **41**, 025002 (2014); arXiv:1412.3277; Phys. Rev. D **91**, 075017 (2015).

[6] K. Doroba, J. Kalinowski, J. Kuczmarski, S. Pokorski, J. Rosiek, M. Szleper, and S. Tkaczyk, Phys. Rev. D **86**, 036011 (2012).

[7] D. A. Dicus and R. Vega, Phys. Rev. Lett. **57**, 1110 (1986); M. J. Duncan, G. L. Kane, and W. W. Repko, Nucl. Phys. **B272**, 517 (1986).

[8] V. D. Barger, K. m. Cheung, T. Han, and R. J. N. Phillips, Phys. Rev. D **42**, 3052 (1990); J. Bagger, V. D. Barger, K. m. Cheung, J. F. Gunion, T. Han, G. A. Ladinsky, R. Rosenfeld, and C.-P. Yuan, Phys. Rev. D **52**, 3878 (1995).

[9] J. Bagger, V. D. Barger, K. m. Cheung, J. F. Gunion, T. Han, G. A. Ladinsky, R. Rosenfeld, and C.-P. Yuan, Phys. Rev. D **52**, 3878 (1995).

[10] J. M. Butterworth, B. E. Cox, and J. R. Forshaw, Phys. Rev. D **65**, 096014 (2002).

[11] A. Alboteanu, W. Kilian, and J. Reuter, J. High Energy Phys. 11 (2008) 010; T. Han, D. Krohn, L. T. Wang, and W. Zhu, J. High Energy Phys. 03 (2010) 082; C. Englert, B. Jager, M. Worek, and D. Zeppenfeld, Phys. Rev. D **80**, 035027 (2009); A. Freitas and J. S. Gainer, Phys. Rev. D **88**, 017302 (2013); W. Kilian, T. Ohl, J. Reuter, and M. Sekulla, Phys. Rev. D **91**, 096007 (2015).

[12] E. Accomando, A. Ballestrero, S. Bolognesi, E. Maina, and C. Mariotti, J. High Energy Phys. 03 (2006) 093; A. Ballestrero, G. Bevilacqua, and E. Maina, J. High Energy Phys. 05 (2009) 015; A. Ballestrero, G. Bevilacqua, D. B. Franzosi, and E. Maina, J. High Energy Phys. 11 (2009) 126.

[13] S. Godfrey, AIP Conf. Proc. **350**, 209 (1995); A. S. Belyaev, O. J. P. Eboli, M. C. Gonzalez-Garcia, J. K. Mizukoshi, S. F. Novaes, and I. Zacharov, Phys. Rev. D **59**, 015022 (1998).

[14] A. Dobado, M. J. Herrero, and J. Terron, Z. Phys. C **50**, 205 (1991); A. Dobado, M. J. Herrero, J. R. Pelaez, E. Ruiz Morales, and M. T. Urdiales, Phys. Lett. B **352**, 400 (1995).

[15] M. Fabbrichesi and L. Vecchi, Phys. Rev. D **76**, 056002 (2007).

[16] I. Brivio, T. Corbett, O. J. P. Èboli, M. B. Gavela, J. Gonzalez-Fraile, M. C. Gonzalez-Garcia, L. Merlo, and S. Rigolin, J. High Energy Phys. 03 (2014) 024.

[17] O. J. P. Eboli, M. C. Gonzalez-Garcia, and J. K. Mizukoshi, Phys. Rev. D **74**, 073005 (2006).
[18] M. Szleper, arXiv:1412.8367.
[19] A. Manohar and H. Georgi, Nucl. Phys. **B234**, 189 (1984); H. Georgi and L. Randall, Nucl. Phys. **B276**, 241 (1986); G. F. Giudice, C. Grojean, A. Pomarol, and R. Rattazzi, J. High Energy Phys. 06 (2007) 045.
[20] K. Hagiwara, S. Ishihara, R. Szalapski, and D. Zeppenfeld, Phys. Lett. B **283**, 353 (1992).
[21] A. Falkowski, F. Riva, and A. Urbano, J. High Energy Phys. 11 (2013) 111.
[22] See, e.g., A. Falkowski and F. Riva, J. High Energy Phys. 02 (2015) 039.
[23] M. Baak *et al.*, arXiv:1310.6708.
[24] J. Elias-Miró, J. R. Espinosa, E. Masso, and A. Pomarol, J. High Energy Phys. 08 (2013) 033.
[25] W. Buchmuller and D. Wyler, Nucl. Phys. **B268**, 621 (1986); B. Grzadkowski, M. Iskrzynski, M. Misiak, and J. Rosiek, J. High Energy Phys. 10 (2010) 085.
[26] S. Schael *et al.* (ALEPH Collaboration), Phys. Lett. B **614**, 7 (2005); P. Achard *et al.* (L3 Collaboration), Phys. Lett. B **586**, 151 (2004); G. Abbiendi *et al.* (OPAL Collaboration), Eur. Phys. J. C **33**, 463 (2004).
[27] V. Khachatryan *et al.* (CMS Collaboration), arXiv: 1507.03268.
[28] S. Chatrchyan *et al.* (CMS Collaboration), Eur. Phys. J. C **73**, 2283 (2013).
[29] G. Aad *et al.* (ATLAS Collaboration), Phys. Rev. Lett. **113**, 141803 (2014); CMS Collaboration, CMS-PAS-SMP-13-015.
[30] ATLAS Collaboration, ATLAS-PHYS-PUB-2012-005.
[31] J. Ellis and T. You, J. High Energy Phys. 06 (2013) 103.
[32] See, for example, CMS Collaboration, arXiv:1307.7135.
[33] T. N. Pham and T. N. Truong, Phys. Rev. D **31**, 3027 (1985); A. Adams, N. Arkani-Hamed, S. Dubovsky, A. Nicolis, and R. Rattazzi, J. High Energy Phys. 10 (2006) 014; J. Distler, B. Grinstein, R. A. Porto, and I. Z. Rothstein, Phys. Rev. Lett. **98**, 041601 (2007); L. Vecchi, J. High Energy Phys. 11 (2007) 054.
[34] N. D. Christensen and C. Duhr, Comput. Phys. Commun. **180**, 1614 (2009).
[35] J. Alwall, M. Herquet, F. Maltoni, O. Mattelaer, and T. Stelzer, J. High Energy Phys. 06 (2011) 128.
[36] T. Sjostrand, S. Mrenna, and P. Z. Skands, J. High Energy Phys. 05 (2006) 026.
[37] J. de Favereau, C. Delaere, P. Demin, A. Giammanco, V. Lemaître, A. Mertens, and M. Selvaggi, J. High Energy Phys. 02 (2014) 057.
[38] J. S. Schwinger, Phys. Rev. **74**, 1439 (1948); S. N. Gupta, Proc. Phys. Soc. London Sect. A **63**, 681 (1950).
[39] M. E. Peskin and T. Takeuchi, Phys. Rev. Lett. **65**, 964 (1990); M. Golden and L. Randall, Nucl. Phys. **B361**, 3 (1991); B. Holdom and J. Terning, Phys. Lett. B **247**, 88 (1990); M. E. Peskin and T. Takeuchi, Phys. Rev. D **46**, 381 (1992); G. Altarelli and R. Barbieri, Phys. Lett. B **253**, 161 (1991); G. Altarelli, R. Barbieri, and S. Jadach, Nucl. Phys. **B369**, 3 (1992); **376**, 444(E) (1992)].
[40] R. Barbieri, A. Pomarol, and R. Rattazzi, Phys. Lett. B **591**, 141 (2004); R. Barbieri, A. Pomarol, R. Rattazzi, and A. Strumia, Nucl. Phys. **B703**, 127 (2004).